Mon. Not. R. astr. Soc. (1980) **191**, 675–684

Seeing-limited radial velocity field mapping of extended emission line sources using a new imaging Fabry–Perot system

Keith Taylor *Royal Greenwich Observatory, Herstmonceux Castle, Hailsham, East Sussex BN27 1RP*

Paul D. Atherton *Imperial College, Prince Consort Road, London SW7 2BZ*

Received 1979 September 5

Summary. TAURUS, a new Fabry–Perot imaging device, designed to obtain complete seeing-limited radial velocity field maps of extended emission-line sources, is described. A servo-controlled Fabry–Perot is used with a focal reducer and a two-dimensional photon-counting (area detector) system, to obtain the velocity information. The system has been fully tested and the first observations of the highly complex velocity field of the irregular galaxy, M82, are used to illustrate the power of the instrument.

1 Introduction

The first results from TAURUS, a new imaging Fabry–Perot (FP) interferometer have been obtained using the RGO 36-in reflector. The instrument is specifically designed to obtain seeing-limited radial velocity field information for extended astronomical emission line sources and utilizes the Image Photon Counting System (IPCS: Boksenberg 1972) as a detector.

The astrophysical motivation behind such a device covers a very broad range of observational astronomy, from the study of planetary nebulae, H II regions and supernova remnants in our own Galaxy, to that of rotation curves and anomalous motions within spiral, irregular, interacting and active galaxies. We see TAURUS as a natural progression in the development of FP systems; it will provide high spatial resolution using area detectors, while employing the flexibility of the servo-stabilized FP technology developed at Imperial College (Hicks, Reay & Scadden 1974).

Piezo-electric scanning has many advantages over the more widely used and simpler technique of pressure scanning. Fundamental amongst these is the ability to alter the wavelength scan range (or free spectral range), $\Delta\lambda$ and hence spectral resolving power, R, by a simple change of the etalon spacing. This flexibility is not accessible to pressure scanning where the scan range is strictly limited by the gas pressure available, and is typically less than 20 Å. For TAURUS, R can be chosen in the range $2\times10^2 \lesssim R \lesssim 10^5$, equivalent to scan ranges of $1000\,\text{Å} > \Delta\lambda > 2\,\text{Å}$, thus allowing us to match the requirements of the particular astrophysical problems to be studied.

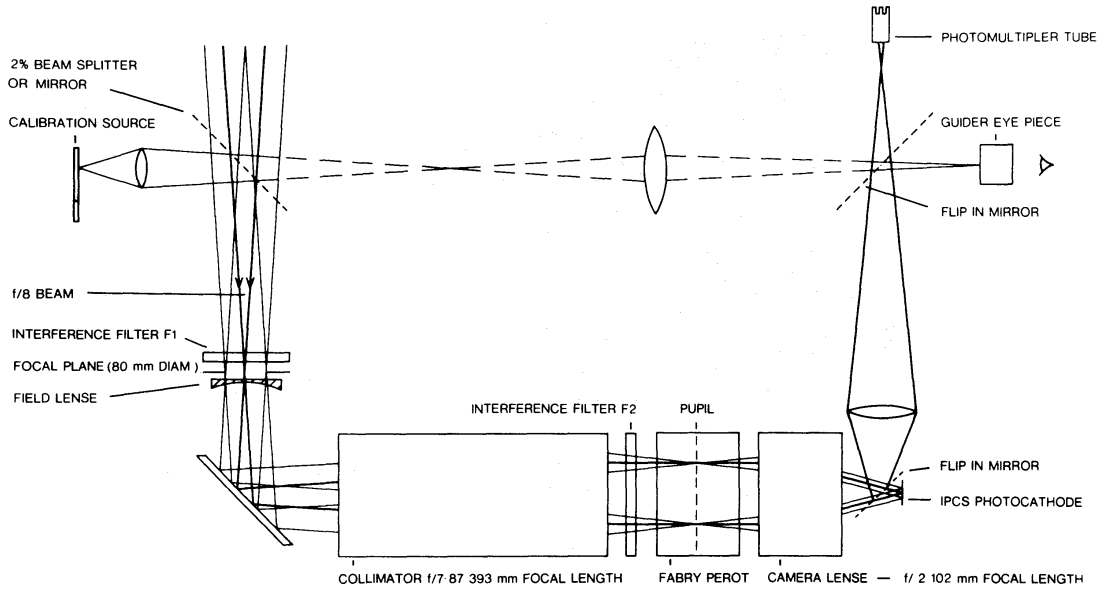

Figure 1. TAURUS: Optical configuration (schematic).

2 Instrumentation

The principal components of the instrument comprise a focal-reducer system, a servo-controlled FP, an order-isolating interference filter, and an Image Photon-Counting System plus subsidiary calibration optics. Fig. 1 gives a schematic representation of the optical layout. Light from the source is imaged by the Cassegrain optics of the telescope on to an iris diaphragm. The light is then collimated, passed through the FP and the source is then re-imaged by the camera lens on to the photocathode of the IPCS. An order sorting interference filter is placed either at the focal plane (F1) or in the collimated beam (F2). The optics thus produce an image of the object, modified by the FP interference fringes. As the FP is scanned these fringes track radially over the entire field of view and allow us to reconstruct the form of the velocity field at each pixel of the image plane.

2.1 FOCAL REDUCER

The collimator/camera optics were designed by C. G. Wynne and C. F. W. Harmer at RGO, and are capable of imaging a 9 arcmin field at the *f*/7.9 Cassegrain focus of the AAT; the 393-mm focal length collimator was specifically constructed by ICOS Ltd. The camera lens is a commercially available Dallmeyer Rareac, 102 mm focal length *f*/2 camera and is shortly to be replaced by a higher performance custom designed version. The focal reducer decreases the input *f*/ratio by a factor of 4, thus giving a scale of 27 arcsec mm^{-1} at the IPCS photocathode at the AAT. The system has been subjected to a full programme of flexure tests on the 36-in telescope at Herstmonceux, no degradation of image quality or shift in position with telescope attitude was found.

2.2 THE FABRY–PEROT

The FP interferometer was designed and built at Imperial College, London. It has an 80-mm working aperture and is piezo-scanned and servo-controlled, using capacitance micrometry to detect deviations from parallelism or changes in the absolute spacing (Hicks *et al.* 1974; Atherton *et al.* 1978). This technique is used in preference to optical methods of servo-stabilization (Ramsey 1962) because in these systems the leakage of light from the optical

reference channel into the signal channel would severely limit the ability of the system to observe faint sources. In practice, the stability of the FP is such that the drift is less than $\lambda/100$, in the plate spacing during the course of several nights in the environment of the 36-in telescope Cassegrain focus.

For the initial observations the $\lambda/200$ etalon plates were coated for the red spectral region and gave a reflectance finesse, N_R, of 15 at Hα, rising to 22 at [O I], λ 6300 and falling off to 10 at [O III], λ 5007; these figures are substantially below the design specification, $N_R \leqslant 35$. The FP gap, l, was, at the time of observation, limited to the range $40\,\mu\text{m} \leqslant l \leqslant 250\,\mu\text{m}$, giving a resolving power range of $1.5 \times 10^3 \lesssim R \lesssim 1.5 \times 10^4$; although, with the addition of new FP etalons, at present under construction, the full range of R ($2 \times 10^2 < R < 10^5$) quoted in the Introduction, will be available to us.

2.3 MICROPROCESSOR CONTROL

The FP is controlled using a Motorola 6800 microprocessor interfaced to our system at RGO by N. M. Parker. Using this system, it is possible to scan the FP and also to change its parallelism, a facility which will allow us to optimize the performance automatically; instructions can be sent to the peripheral calibration lamps, mirrors, shutters and filter slides for this purpose. The microprocessor also enables us to interface TAURUS with the IPCS or any other detector control system, such that the detector frame readout may be synchronized with the FP scans.

2.4 THE DETECTOR

During various test runs on the 36-in telescope and INT at RGO, we have used photographic plates (IIIaJ), the 40-mm McMullan electronographic camera and an IPCS; indeed a wide variety of area detectors could be interfaced to TAURUS. However, for reasons of availability, sensitivity and flexibility in data acquisition and display, the IPCS is seen to be the principal detector for the immediate future.

The use of relatively large pixels (55–110 μm) allows us to bypass the event centring logic (ECD), which is the major limitation to the photon arrival rate, thus enabling a count rate of ~ 0.5 count pixel^{-1}, frame^{-1}, or in this case ~ 25 count pixel^{-1} s^{-1} to be tolerated without severe loss of linearity.

We should emphasize here that since our main aim is to obtain velocity information as opposed to photometric data, non-linearity of the detector is not a severe problem, and by using the IPCS in this manner, the effective dynamic range (previously its major limitation) is significantly increased.

2.5 ADVANTAGES OVER COMPETING DEVICES

The methods by which one can usefully compare competing dispersive systems have been discussed by many authors (Meaburn 1976; Jacquinot 1960 and references therein). We wish here to clarify the arguments by concentrating individually on just those devices which are, at present, being used or proposed for seeing limited extended emission line velocity field studies.

The majority of extragalactic work has used long-split spectroscopy. Such high resolution studies would use, typically, a 25 Å mm^{-1} dispersion to obtain velocity resolutions of ~ 30 km s^{-1} for a slit of 1 arcsec width and 2 arcmin length with a 4-m aperture telescope (Van der Kruit 1975; Goad, de Veny & Goad 1979).

TAURUS, on the other hand, using the same 4-m telescope can access a 9 arcmin field, giving it a spatial gain of ~2000. However, N_R separate FP frames (where the finesse N_R is typically ~25) have to be accumulated before the complete velocity information for one emission line has been achieved; hence reducing the effective gain to ~80. In addition the spectrograph will allow several emission lines to be studied simultaneously; in general a maximum of three to five lines are used as velocity indicators (Hα, [N II] and [S II], for example). Hence, assuming the total optical efficiencies of the grating and TAURUS are similar, a practical gain of ~20 in observing time required to access the same information, is achieved over the grating techniques.

TAURUS has a further advantage in that it does not lose speed in conditions of poor seeing, whereas much light is generally lost at the slit jaws of spectrographs in all but the best observational conditions.

More recent work of this type has used the FP interferogram technique (Tully 1974; de Vaucouleurs, de Vaucouleurs & Pence 1974). TAURUS, in a strictly optical sense, is very similar to these devices in that the information throughput (or luminosity) is approximately equivalent. For the interferogram case, the variations in the radii of the FP fringe pattern are used to identify the velocity. This method, however, suffers a severe problem. There is ambiguity in the results which means that all data close to high intensity knots of emission have to be excluded. This is rather unfortunate in many extragalactic applications of the technique since, for example, H II regions appear generally as 'beads on a string' along spiral arms and hence much of the important, high intensity small scale structure is lost. In such situations seeing limited resolution is of paramount importance.

By scanning the FP in the manner used by TAURUS these problems are overcome and we are able to obtain unambiguous velocity field information. TAURUS has the added advantage over both the long slit spectrograph and the interferogram method in that, rather than sampling only a small, subjectively selected subset of the image it allows the velocity mapping of a whole field to be accumulated. In this way, for example, the velocity field of all visible H II regions in a galaxy can be obtained rather than those that by chance happen to coincide with the long slit position or the interferogram fringe pattern.

3 Field limitations

In practice, the full field angle, β, subtended on the sky, is constrained by the following considerations.

3.1 PARAMETERS OF THE DETECTOR

Consider the use of TAURUS at a telescope of diameter, D, with an output camera lens focal ratio, F_0. The pixel size, ϵ, of the area detector will define the spatial resolution, α, within the field angle β, which is itself constrained by the number, p, of detector pixels, such that

$$\beta_0 = \alpha\sqrt{p} = \epsilon\sqrt{p}/DF_0. \tag{1}$$

For example to match the device to both the AAT and the IPCS ($\epsilon \sim 75\,\mu$m), an output focal ratio $F_0 \sim 2$ is required to obtain seeing-limited ($\alpha \sim 2$ arcsec) resolution. This implies that a field $\beta \sim 15$ arcmin could be accessed using the IPCS extended memory ($p \sim 192\,000$ pixels).

3.2 ACCEPTANCE ANGLE OF INTERFERENCE FILTER

In general the emission-line radial velocity fields will be mapped for objects whose lines are relatively strong compared to the continuum. This can be regarded as the 'weak continuum' case; here, several FP orders can be included in the band-pass of the interference filter and the field will not, in general, be limited by its acceptance angle.

However, for the 'strong continuum' case, it is important to limit the band-pass, $\Delta\lambda_F$ of the filter (centred at λ_0), so that only a single FP order, n (where $n\lambda = 2l$) is transmitted, giving the constraint

$$\Delta\lambda_F \leqslant \lambda_0/n. \tag{2}$$

The width of the filter, $\Delta\lambda_F$ and hence its acceptance angle can now be an important limitation to the field size.

If the interference filter is placed in the Cassegrain focal plane (position F1; Fig. 1), whose input focal ratio is F_I, the field angle is simply defined by the diameter, d_F, of the filter. Hence

$$\beta_{F1} \leqslant d_F/F_I D. \tag{3}$$

However, in this condition, the band-pass, $\Delta\lambda_F$ has a lower limit given by

$$\Delta\lambda_F > \lambda_0/8F_I^2. \tag{4}$$

As an example, the $f/7.9$ Cassegrain focus of the AAT limits $\Delta\lambda_F$ to above 13 Å for $\lambda_0 \sim 6000$ Å, which in turn, implies that $R < 1.2 \times 10^4$ for $N_R \sim 25$. For higher spectral resolutions the interference filters must be placed in the collimated beam (position F2; Fig. 1).

Here the field itself is limited by the acceptance angle such that:

$$\beta_{F2} \leqslant (8d^2/nD^2)^{1/2} \tag{5}$$

where d is the diameter of the on-axis collimated beam. It should be noted that this limitation is 'soft' in that the effect of the filter transmission blue-shift with increasing field angle can, to a degree, be removed by calibration. However, in cases where there is a choice it is desirable to place the filter in the focal plane, since the systematic changes in spectral response across the field are negligible for this position.

3.3 WAVELENGTH CHANGE ACROSS ONE PIXEL

If each pixel is to represent a unique spectral element, such that the change in wavelength across a pixel can be neglected,

$$\beta_A \leqslant 2d^2/\alpha RD^2. \tag{6}$$

For larger fields than this the spectral resolution or effective finesse of the system is degraded accordingly.

3.4 COLLIMATION

The size, complexity and cost of the collimator all increase rapidly with field size and hence a compromise between good quality image reproduction over a large wavelength range and field size must be obtained. This involves to some extent a non-quantifiable decision, how-

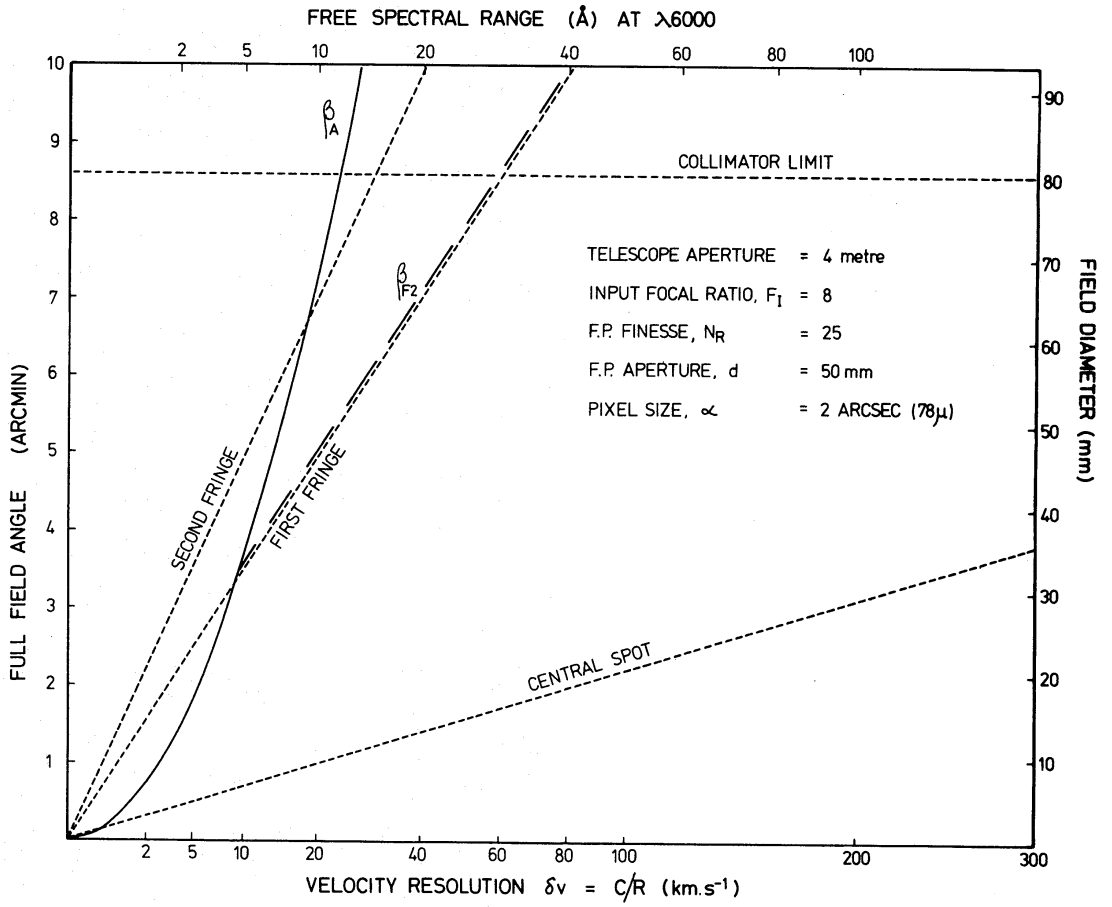

Figure 2. Field angle constraints.

ever, a maximum field size of 9 arcmin at the $f/7.9$ Cassegrain focus of the AAT is more than adequate for almost all astrophysical problems suitable for TAURUS.

The field angle constraints outlined above are diagrammatically represented in Fig. 2 for the design parameters of the system, in an example where it is to be used at an $f/8$ Cassegrain focus of a 4-m telescope with an IPCS pixel size of 75 μm.

The severest constraint at high R is that due to wavelength change across one pixel, however, the allowed field, β_A, given in equation (6) is still more than five times the diameter of the central spot (Jacquinot criteria), at $R \sim 6 \times 10^4$. At intermediate resolutions the interference filter acceptance angle becomes the dominant constraint, while at the lowest R, detector collimator considerations predominate. It should be noted that the FP is always used on axis so as to maximize field angle, β_A, for a given resolving power; the field corresponding to the first two rings of the interference fringe pattern are shown for comparison in the figure.

4 Data acquisition and reduction

Although the method used for obtaining velocity field measures is, in essence the interferogram technique, whereby the image of the object to be studied is superimposed on the FP fringe pattern at the detector, unlike the interferogram method we do not use the deviations from circularity of the fringes to obtain the velocity. Instead, the fringe pattern is scanned and recorded at each independent velocity interval throughout the free spectral range. Hence we obtain independent velocity profiles for each pixel of the image, without encountering

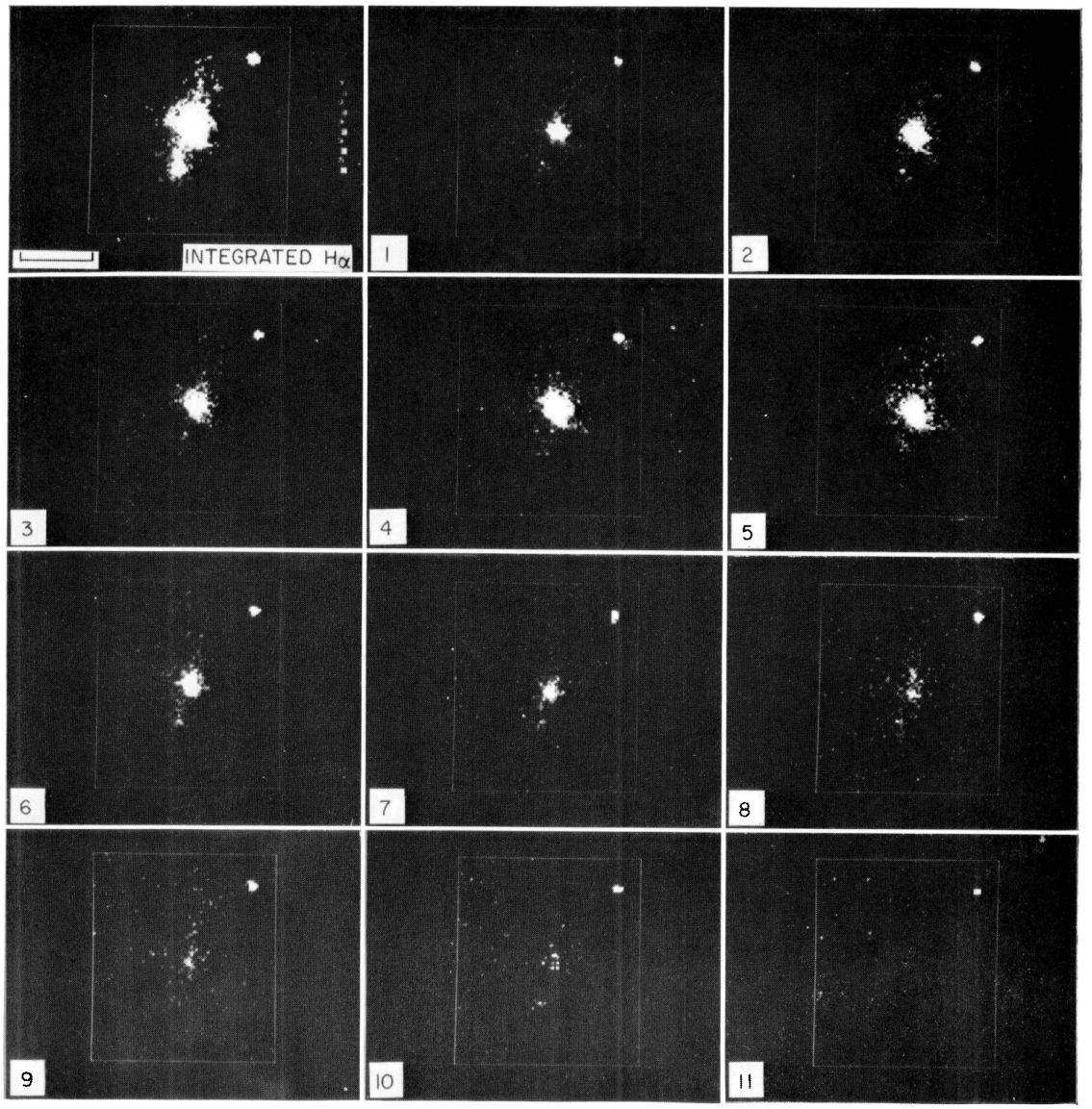

Plate 1. The raw HαFP frames are shown numbered in sequence. No unique velocity can be ascribed to these since they are uncorrected for phase. The first picture is an image formed by summing all separate FP frames (the scale bar is 2 arcmin; top is west and left is north), and is essentially a 10 Å band-width IPCS direct image of the Hα emission in M82.

[*facing page* 680]

the intensity/wavelength ambiguity inherent in the interferogram technique. We thus obtain a full three-dimensional array of data: two dimensions of space and one dimension of velocity (or wavelength).

The fact that we are, in general, observing a field which incorporates a region of the FP fringe pattern larger than the Jacquinot central spot, requires that we correct for this effect; equivalent to a change in the zero point of the wavelength coordinate for each pixel. This zero point variation we term the phase and the many separate velocity profiles cannot be calibrated in wavelength until a map of the phase change from pixel to pixel is achieved.

A phase-map is obtained simply by illuminating the entrance aperture of TAURUS with a monochromatic calibration line source and performing a complete three-dimensional scan. By determining the maximum in the wavelength dimension for each pixel, the phase map can be reconstructed.

We define a complete three-dimensional FP data set for an object as $I(x,y,z)$ which represents the variations in intensity, I, as a function of x,y, the spatial coordinates and z, the etalon gap (z varies by half a wavelength for one FP order to be scanned).

This three-dimensional array may now be reorganized into independent one-dimensional scans, $I_{xy}(z)$ for each pixel (x, y). By utilizing the phase map, these individual scans can be wavelength calibrated to give the set, $I_{xy}(\lambda)$, and hence a mapping of the velocity field of the object is achieved.

Finally by rearranging the set of $I_{xy}(\lambda)$, individual two-dimensional images of the object, $I_\lambda(x,y)$ can be obtained which display its spatial structure as a function of wavelength. Seen in this way, TAURUS is effectively a simple tunable filter allowing us to view the appearance of an object at many separate, line-of-sight, velocities.

Now since each $I_z(x,y)$ FP frame is obtained sequentially, there is a need for some form of relative flux calibration, so that the N_R independent frames can be stacked in the z-direction to form $I(x,y,z)$.

This is achieved in either of two ways. First, a photomultiplier monitor channel is fed approximately 2 per cent of the incident light in the field of view from a beam splitter (Fig. 1), placed before the Cassegrain focus. By synchronizing the integration periods in both the main IPCS channel and the monitor channel, we are able to remove atmospheric transparency effects throughout a scan. Alternatively, any unsaturated stellar image within the IPCS field can be used for the same purpose, provided its spectrum contains no emission or absorption bands within the band-pass of the interference filter.

Lastly, the pixel to pixel sensitivity variations of the IPCS plus interference filter combination, have to be removed. This is usually termed 'flat-fielding' an image, whereby a white light source is used to illuminate evenly the entrance aperture. The IPCS image of this flat field is then used to calibrate pixel sensitivity.

5 Initial results

The emission-line velocity field of M82 has been studied spectroscopically since the fundamental work of Lynds & Sandage (1963). However, it was not until very recently that the complex split-line regions in the minor axis filaments were discovered by Axon & Taylor (1978), which has led to a regeneration of interest in the possibility of explosive events occurring in the nucleus of his enigmatic galaxy. We should note here that it has taken approximately 20 yr to isolate this split line region spectroscopically and we take this as strong support for the need for velocity mapping of the complete field made available by TAURUS.

For these reasons M82 was regarded as a prime candidate for study, and late in the

night of 1979 April 18, we made use of a rare clear period at the 36-in reflector at Herstmonceux to scan the Hα line over a 6.4 arcmin field containing M82.

The finesse of the FP was as described in Section 2 and an etalon spacing of 210 μm was used giving as a spectral resolving power, $R \sim 10^4$ and a scan range of 470 km s^{-1}. An integration time of 500 s was used for each FP frame and 11 frames, separated in wavelength by the 30 km s^{-1} velocity resolution of the FP, were accumulated before twilight forced us to stop. The IPCS was used in a 512 line by 130 increment mode giving a pixel size of ~50 μm square (equivalent to ~3 arcsec on the object), and a 128 x 128 subset of this was recorded in the IPCS memory.

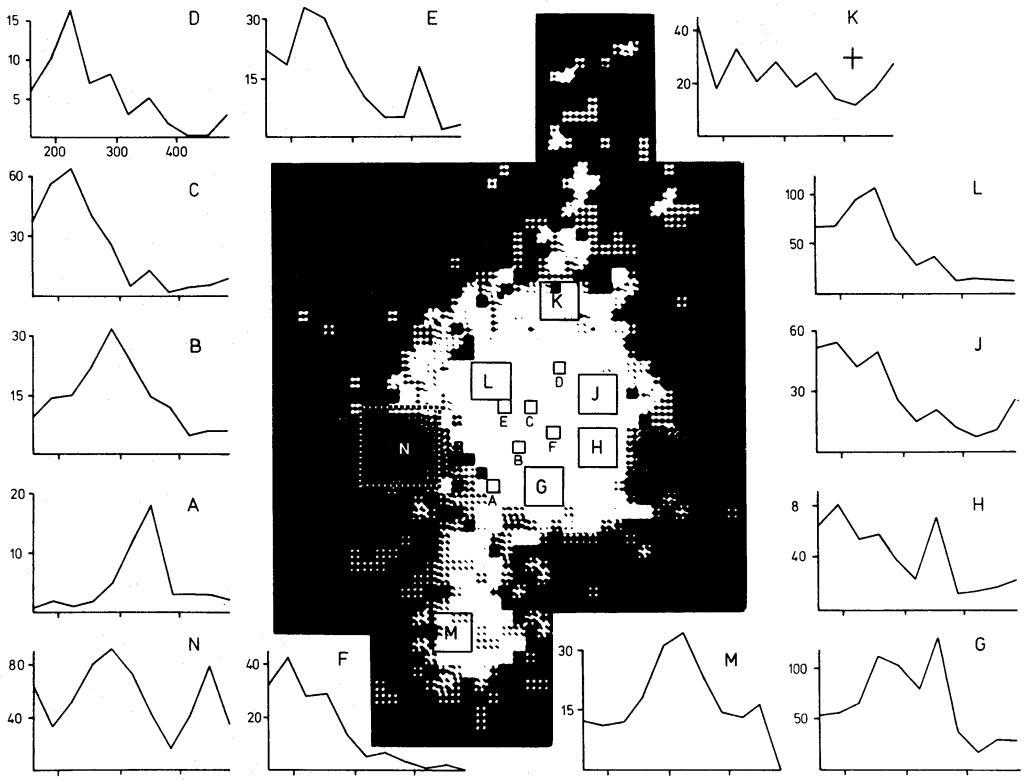

Figure 3. Hα velocity profile from various regions of M82 are shown superimposed on the integrated Hα image. The small squares, regions A–F, represent a single 3 arcsec pixel of the image; the large solid squares, regions K–M, are of dimension 9 arcsec; region N represents an 18 arcsec square over which the velocity profile has been integrated. The accumulated counts for each pixel sample are given on the abscissa axis and the velocity samples have been taken at 32.5 km s^{-1} interval.

The 11 frames are reproduced in Plate 1, together with an integrated Hα image formed by summing all separate FP frames. Structural changes in the minor axis filaments are clearly visible in the separate Hα velocity frames and indeed some of this structure is not seen on any other narrow band image of this object.

Although we have not achieved a complete set of $I_z(x,y)$ frames in this case, we are still able partially to reduce the velocity data through phase correction, as described in Section 4. A sequence of velocity profiles so obtained, is shown in Fig. 3. The truncation of the profiles to the blue of the main peak is due to the incompleteness of the data set; however, we are still able to obtain velocity measures from these crude first results and our S/N ratio is sufficient to identify such velocities for more than 400 separate regions of the galaxy. The results are seen to be in substantial agreement with the velocity map of Heckathorn (1972).

Table 1.

Object	Location in object	Emission line	Line flux (erg s^{-1} cm^{-2} sr^{-1})	Ref.	Resolving power $R = \lambda/\delta\lambda$	Maximum field angle β (arcmin)	Spatial resolution (arcsec^2)	Estimated exposure time (s)
NGC 7293 'Helix Nebula'	Ring	[O I] λ 6300	5×10^{-6}	1	5×10^{4}	2.2	$2\times10^{\star}$	5×10^{3}
A 0034 – 35 'Cartwheel Galaxy'	Spokes and rings	Hβ	$<5\times10^{-6}$	2	2×10^{4}	5.5	2 × 2	2×10^{3}
M1 'Crab Nebula'	Filaments	[O III] λ 5007	3×10^{-5}	3	5×10^{3}	8.6	2 × 2	4×10^{2}
NGC 1275	Low velocity filaments	Hα	5×10^{-6}	4	5×10^{3}	8.6	2 × 2	2×10^{3}
	High velocity filaments	Hα	3×10^{-6}	4	2×10^{3}	8.6	2 × 2	4×10^{3}

★ Individual condensations have dimension 2 × 10 arcsec² (Vorontsov-Velyaminov 1968).

(1) Kaler (1976); Perak & Kohoutek (1967); Taylor (1977).
(2) D. H. Clark, P. G. Murdin & I. J. Danziger (1979, private communication).
(3) Fosbury & Hawarden (1977).
(4) Kent & Sargent (1979).

Discussion

The detective quantum efficiency (DQE) of the TAURUS, IPCS combination, as defined by the product of the efficiencies in the optical chain and the quantum efficiency of the detector, was determined by scanning a field containing a star of known visual magnitude and comparing the counts obtained with previous DQE determinations made with the IPCS in direct mode at the AAT, using only a Johnson V-band filter between the telescope and the detector. In this manner the efficiency of the optics of TAURUS was estimated at approximately 0.2 ± 0.1, where the large estimated error is a result of uncertainties in the telescope efficiency and those due to transforming from broad to narrow band measurements. The measured optical efficiency of 20 per cent compares very well with that calculated from the light losses at glass/air interfaces and at the FP and interference filter, and implies a combined DQE of approximately 1 per cent at Hα when the IPCS is included.

Since this is a measured efficiency obtained in less than optimal observing conditions, it is instructive to use it in calculating what might be practically achieved at the $f/8$ focus of a typical 4-m telescope.

Using a finesse N_R of 25 (implying the need for 25 independent FP frames, $I_z(x,y)$, to achieve a complete velocity map), a total exposure time of 10^4 s should enable us to obtain Hα velocity field information ($S/N \sim 5$), with a 2 arcsec pixel, down to a limit in surface brightness of 2.5×10^{-6} erg cm^{-2} s^{-1} sr^{-1} within the wavelength resolution element $\delta\lambda$ defined by R. This is to be compared with the Hα surface brightness of 2.5–5.5×10^{-6} erg cm^{-2} s^{-1} sr^{-1} for the faintest diffuse emission observable on the red Palomar Sky Survey plates (Peimbert, Rayo & Torres-Peimbert 1975).

This gives an idea of the power of the system. Most emission-line nebulae and galaxies, visible on the Sky Survey will be accessible to TAURUS at a moderate spectral resolution.

As a guide to the potential of the system, we have estimated exposure times ($S/N \sim 5$) and field sizes for a few cases of particular astronomical interest using a 4-m telescope. The results are presented in Table 1.

The instrument is now fully commissioned and is at present being upgraded to allow complete remote control of all facilities (mirrors, shutters, calibration sources, etc.) to optimize the use of telescope time and simplify the operation for the general user.

References

Atherton, P. D., Hicks, T. R., Reay, N. K. & Wells, M., 1978. *Proceedings of the 4th International Colloquium on Astrophysics,* Trieste, ed. Hack, M.

Axon, D. J. & Taylor, K., 1978. *Nature,* **274**, 37.

Boksenberg, A., 1972. *Auxiliary Instrumentation for Large Telescopes,* p. 205, Proceedings of ESO/CERN Conference, Geneva.

Fosbury, R. A. E. & Hawarden, T. G., 1977. *Mon. Not. R. astr. Soc.,* **178**, 473.

Goad, J. W., de Veny, J. B. & Goad, L. E., 1979. *Astrophys. J. Suppl.,* **39**, 439.

Heckathorn, H. M., 1972. *Astrophys. J.,* **173**, 501.

Hicks, T. R., Reay, N. K. & Scaddan, R. J., 1974. *J. Phys. E. Sci. Instrum.,* **7**, 27.

Jacquinot, P., 1960. *Rep. Progr. Phys.,* **24**, 267.

Kaler, J. B., 1976. *Astrophys. J. Suppl.,* **31**, 517.

Kent, S. M. & Sargent, W. L. W., 1979. *Astrophys. J.,* **230**, 667.

Lynds, C. R. & Sandage, A. R., 1963. *Astrophys. J.,* **137**, 1005.

Meaburn, J., 1976. *Detection and Spectroscopy of Faint Light,* Reidel, Dordrecht.

Peimbert, M., Rayo, J. F. & Torres-Peimbert, S., 1975. *Rev. Mex. Astr. Astrofis.,* **1**, 289.

Ramsey, J. V., 1962. *Appl. Opt.,* **1**, 411.

Taylor, K., 1977. *Mon. Not. R. astr. Soc.,* **181**, 475.

Tully, R. B., 1974. *Astrophys. J. Suppl.,* **27**, 415.

Van der Kruit, P. C., 1975. *Astrophys. J.,* **195**, 611.

de Vaucouleurs, G., de Vaucouleurs, A. & Pence, W., 1974. *Astrophys. J.,* **194**, L119.